Optical Mode Entanglement Generation from an Optomechanical Nanobeam

Qi-Zhi Cai(蔡淇智)[1,3†], Bo-Yu Fan(樊博宇)[1,2,6†*], Yun-Ru Fan(范云茹)[1,3], Guang-Wei Deng(邓光伟)[1,3], You Wang(王淞)[1,4], Hai-Zhi Song(宋海智)[1,4], Guang-Can Guo(郭光灿)[1,2,3,5,6], and Qiang Zhou(周强)[1,2,3,5,6*]

[1]*Institute of Fundamental and Frontier Sciences, University of Electronic Science and Technology of China, Chengdu 611731, China*
[2]*Center for Quantum Internet, Tianfu Jiangxi Laboratory, Chengdu 641419, China*
[3]*Key Laboratory of Quantum Physics and Photonic Quantum Information (Ministry of Education), University of Electronic Science and Technology of China, Chengdu 611731, China*
[4]*Southwest Institute of Technical Physics, Chengdu 610041, China*
[5]*CAS Key Laboratory of Quantum Information, University of Science and Technology of China, Hefei 230026, China*
[6]*Jiangxi Research Institute, University of Electronic Science and Technology of China, Chengdu 641419, China*

(Received 11 July 2024; accepted manuscript online 25 September 2024)

Nano-optomechanical systems, capable of supporting enhanced light-matter interactions, have wide applications in studying quantum entanglement and quantum information processors. Yet, preparing optical telecom-band entanglement within a single optomechanical nanobeam remains blank. We propose and design a triply resonant optomechanical nanobeam to generate steady-state entangled propagating optical modes and present its quantum-enhanced performance for teleportation-based quantum state transfer under realistic conditions. Remarkably, the entanglement quantified by logarithmic negativity can obtain $E_{\mathrm{N}} = 1$. Furthermore, with structural imperfections induced by realistic fabrication processes considered, the device still shows great robustness. Together with quantum interfaces between mechanical motion and solid-state qubit processors, the proposed device potentially paves the way for versatile nodes in long-distance quantum networks.

DOI: 10.1088/0256-307X/41/11/114201

Entanglement is a crucial resource for modern quantum technologies,[1] in which the entanglement between lights, as the only traveling information carrier within long-distance quantum networks,[2] plays an essential role in practical quantum information processing.[3–15] For the relevant candidate platforms, the optomechanical system has become one of the research frontiers and hotspots in recent decades,[16,17] due to its ability to couple mechanical motion to a variety of natural or engineered quantum systems[18,19] paving a path toward generating entanglement between them.[20–30] Across multiple designs of optomechanical systems, the photonic crystal nanobeam shows the merit of nanoscale integration, enhanced light-matter interactions, and gigahertz mechanical resonance frequencies that allow direct access to the quantum ground state,[31–33] making it a promising toolbox for quantum state engineering[34] and quantum technologies such as optical wavelength converters[35] and microwave entanglers.[20] Despite the growing demand for multimode quantum information processors, only a few reports have demonstrated the entanglement of even two optical modes generated from a single optomechanical nanobeam. This limitation is primarily due to the trade-off between achieving a small free spectral range, required for efficient spectrum utilization, and maintaining high-quality factors, essential for strong optomechanical interactions.[36–38] Note that the zipper optomechanical cavity has emerged as a promising solution to address these competing requirements.[39–41]

In this work, we directly design a single nanobeam with two optical transverse-electric (TE) resonant modes instead of the zipper optomechanical cavity to generate entanglement between two optical telecom-band modes by manipulating the structural spatial distribution perturbatively via finite element methods. The device parameters are meticulously designed to balance the enhanced optical quality factors and appropriate operating frequencies while maintaining the mechanical quality factor and resonance frequency within a stable range. Despite a 7.6 THz frequency deviation between the two optical resonances due to the band gap edges of the nanobeam, the flexible geometry paves a path toward spectrum manipulation in both coarse and refined ways. Through standard Langevin equations and input-output formalism, the entanglement can obtain $E_{\mathrm{N}} = 1$ quantified by logarithmic negativity. Taking the example of teleportation-based communication in an application scenario, we show its performance as quantified by the quantum state transfer fidelities for a typical coherent-squeezed state, i.e., $|\alpha, r\rangle = |2, 0.5\rangle$ with coherent state amplitude α and squeezing parameter r.

†Qizhi Cai and Boyu Fan contributed equally to this work.
*Corresponding authors. Email: fby@uestc.edu.cn; zhouqiang@uestc.edu.cn
© 2024 Chinese Physical Society and IOP Publishing Ltd

The classical threshold of teleportation fidelity of a pure coherent state is 0.5,[42] indicating that the proposed entangler can act as a repeater node in long-distance quantum networks with fidelity $F = 0.6$.[43] Moreover, we analyze the robustness of the entanglement by considering structural imperfections in finite element simulations,[44] the results represent that the percentage of devices in the resolved-sideband regime is 91%, in which all the devices can still maintain $E_{\mathrm{N}} > 0.9$, showing the robustness of our design regarding to the fabrication processes.

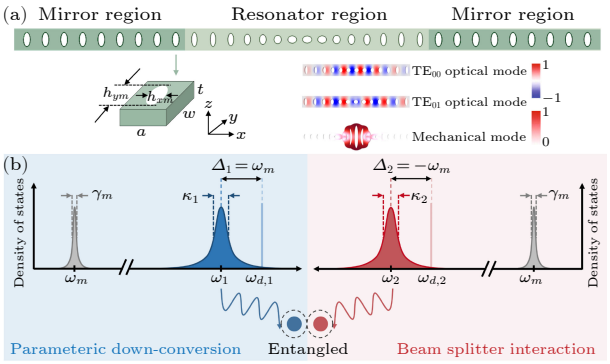

Fig. 1. (a) Schematic diagram of the optomechanical nanobeam cavity and unit cell geometry in the mirror region as well as the finite-element simulations of the device. The h_{xm} and h_{ym} correspond to the width and length of the hole in the nanobeam; a, w, and t are the length, width, and height of the hole unit. The E_y components of the TE_{00} and TE_{01} optical modes (top and middle) are shown alongside the displacement field of the co-localized mechanical mode (bottom). (b) The photon–phonon interaction pictures of the optical and mechanical oscillators with resonant frequencies ω_m and ω_j for parametric down-conversion and beam splitter interaction processes, respectively. Each optical cavity is driven by coherent tone with $\omega_{d,\,j} = \omega_j \pm \omega_m$ on the blue and red sidebands. In the parametric down-conversion process, a photon from the coherent tone with $\omega_{d,\,1}$ is converted to a photon in the TE_{00} mode with ω_1 and a phonon with ω_m in the mechanical mode. In the beam splitter interaction process, a phonon in the mechanical mode absorbs a photon from the coherent tone with $\omega_{d,\,2}$ to generate a photon in the TE_{01} mode. The photons in TE_{00} and TE_{01} modes get entangled in certain conditions.

Hamiltonian and Dynamics of the System. As schematically shown in Fig. 1, the system contains a mechanical mode with angular resonance frequency ω_m and intrinsic damping rate γ_m to two optical modes (angular resonance frequency ω_j, total damping rates $\kappa_j = \kappa_{\mathrm{in},\,j} + \kappa_{\mathrm{ex},\,j}$ with internal loss $\kappa_{\mathrm{in},\,j}$ and input-port coupling rates $\kappa_{\mathrm{ex},\,j}$, $j = 1$ and 2 correspond to TE_{00} and TE_{01} modes) with single-photon coupling rate $g_{0,\,j}$. The two optical modes exert radiation pressure on the mechanical resonator. In return, the mechanical breathing mode of the mechanical resonator mediates a retarded interaction between the optical modes. In the presence of strong optical pumps, the system can be linearized and described in the frame rotating at angular frequencies ω_j and ω_m with the Hamiltonian[45]

$$\hat{H} = \hbar G_1(\hat{c}_1\hat{b} + \hat{b}^\dagger\hat{c}_1^\dagger) + \hbar G_2(\hat{c}_2\hat{b}^\dagger + \hat{b}\hat{c}_2^\dagger), \tag{1}$$

where $\hat{c}_j$ and $\hat{b}$ are the annihilation operators of the optical cavity j and the mechanical resonator, $G_j = g_{0,\,j}\sqrt{n_j}$ is the cavity-enhanced optomechanical coupling; n_j is the average photon number of mode j due to the blue- and red-detuned drives in the resolved-sideband regime ($\omega_m > \kappa_1, \kappa_2$), with detuning $\Delta_j = \omega_{d,\,j} - \omega_j = \pm\omega_m$, which allows neglecting the fast-oscillating terms. From Eq. (1), the first term describes a parametric down-conversion interaction that generates entanglement between phonons and photons in TE_{00} mode. The second term represents an interaction of a beam splitter so that the excitations are exchanged between phonons and photons in TE_{01} mode. As shown in Fig. 1(b), suppose that the optomechanical coupling rate $4G_j^2/\kappa_j$ exceeds the mechanical resonator's decoherence rate $\gamma_m\bar{n}_m$, with bath occupancy $\bar{n}_m = [e^{\hbar\omega_m/k_{\mathrm{B}}T} - 1]^{-1}$ (k_{B} is Boltzmann's constant and T is the device temperature), the two output fields are mapped into a two-mode squeezed state.[20,46]

The output propagating optical modes $\hat{d}_j$ can be expressed by the quantum noise operators $\hat{c}_{j,\,\mathrm{ex}}$ and $\hat{c}_{j,\,\mathrm{in}}$, corresponding to the optical resonators' input fluctuations and the intrinsic losses of the optical modes, as well as the quantum Brownian noise operator $\hat{b}_{\mathrm{in}}$, reading[45]

$$\begin{aligned}\hat{d}_1 &= \alpha_1\hat{c}_{1,\mathrm{ex}} + \alpha_{12}\hat{c}_{2,\mathrm{ex}}^\dagger + \alpha_{1m}\hat{b}_{\mathrm{in}}^\dagger \\ &\quad + \alpha_{1,\mathrm{in}}\hat{c}_{1,\mathrm{in}} + \alpha_{12,\mathrm{in}}\hat{c}_{2,\mathrm{in}}^\dagger, \\ \hat{d}_2 &= \alpha_{21}\hat{c}_{1,\mathrm{ex}}^\dagger + \alpha_2\hat{c}_{2,\mathrm{ex}} + \alpha_{2m}\hat{b}_{\mathrm{in}} \\ &\quad + \alpha_{21,\mathrm{in}}\hat{c}_{1,\mathrm{in}}^\dagger + \alpha_{2,\mathrm{in}}\hat{c}_{2,\mathrm{in}},\end{aligned} \tag{2}$$

where the parameters mainly decided by the optomechanical cooperativity $\Gamma_j = 4G_j^2/\kappa_j\gamma_m$ are explicitly given in the Supplementary Material.[45]

Device Implementation and Numerical Analysis. As shown in Fig. 1(a), the proposed system is based on a multimode optomechanical nanobeam cavity, including an integrated optical and mechanical nanoscale resonator within two mirror regions.[45] The taper sections are treated as reflectors to confine the optical modes and fundamental mechanical mode, by varying lattice spacing and ellipse dimensions simultaneously from resonator to mirror region, i.e., h_{xm}, h_{ym}, w, and a. Combining previously reported single-mode nanobeam[47] and structure disturbance in resonator region,[38] the TE_{00} and TE_{01} modes at telecom-band can be achieved by modifying electric field profiles of air and dielectric modes.

There are five parameters determined through device design for quantifying the entanglement, i.e., intrinsic optical quality factors $Q_{\mathrm{in},\,j}$, mechanical quality factor Q_m, mechanical resonance frequency ω_m, optical resonance frequency ω_j and single-photon coupling $g_{0,\,j}$. Note that a strong photon–phonon interaction for entanglement generation accords with a high $Q_{\mathrm{in},\,j}$,[47] which meanwhile will hamper the output of the entangled fields. Moreover, to realize high $Q_{\mathrm{in},\,j}$ and $g_{0,\,j}$, the corresponding structural design will induce a large frequency difference between the TE_{00} and TE_{01} modes.[48] In addition, the optical resonators considered in this work are in the resolved-sideband regime, which also requires an enhanced optical quality factor. With comprehensive consideration, $Q_{\mathrm{in},\,j}$ of

the demonstrated device is set to 10^5–10^6 with a free spectral range of about 7.6 THz.[20,49] It is worthy to mention that Q_m, ω_m and $g_{0,j}/2\pi$ can keep approximately stable during the structural manipulation, therefore, Q_m is designed with the order of 10^8 for high cooperativities, which is valid and certified by recent experimental work.[50] Here, $\omega_m/2\pi = 5.35$ GHz, and the $g_{0,j}/2\pi$ values for TE_{00} and TE_{01} modes are $\sim 9.77 \times 10^5$ and $\sim 2.01 \times 10^5$ Hz, respectively.

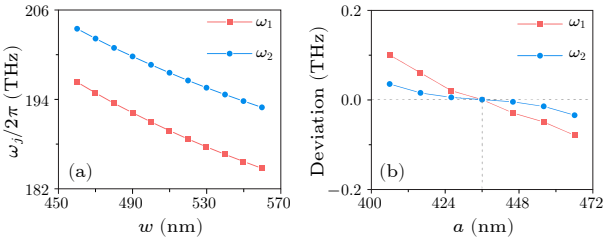

Fig. 2. (a) Optical angular resonance frequencies ω_j versus the width of the hole unit w, with $a = 436$ nm. (b) Compared to the device with $a = 436$ nm, the frequency deviation of each device with different a versus a, in which $w = 500$ nm.

To utilize the spectrum efficiently, the relationship between ω_j and structural parameters is presented. One can find that the variation of width w induces a coarse frequency modulation as shown in Fig. 2(a), with a slope of approximately 0.12 THz/nm. Relatively, a refined modulation could be achieved by changing lattice spacing a from Fig. 2(b), where the resonance frequencies can be modulated via the approximate slope of ~ 3 GHz/nm for ω_1 and ~ 1.2 GHz/nm for ω_2. These results provide a natural way to form an integrated device array and make the operating frequency flexibly tuned.[51] Considering the resonance frequencies ω_j near the optical telecom-C band, we choose the device with $w = 500$ nm and $a = 436$ nm for the following results.

Results. To verify the quantum correlation, two-mode squeezing can be intuitively visualized via the quasiprobability Wigner function

$$W(v) = \frac{\exp[-\frac{1}{2}(v^\dagger V^{-1} v)]}{\pi^2 \sqrt{\det(V)}}, \tag{3}$$

where V is a 4×4 covariance matrix that completely characterizes the propagating output fields, with elements $V_{kl} = \langle \delta v_k \delta v_l + \delta v_l \delta v_k \rangle / 2$, $\delta v_k = v_k - \langle v_k \rangle$, and $v = [\hat{X}_1, \hat{Y}_1, \hat{X}_2, \hat{Y}_2]^T$. The quadratures are defined as $\hat{X}_j = (\hat{d}_j + \hat{d}_j^\dagger)/\sqrt{2}$ and $\hat{Y}_j = (\hat{d}_j - \hat{d}_j^\dagger)/i\sqrt{2}$.[45] Different marginals of the Wigner function are presented in Fig. 3, wherein the complementary variables are integrated. The quadrature marginals from the same optical mode $\{X_1, Y_1\}$ and $\{X_2, Y_2\}$ show uncorrelated thermal noise above the vacuum noise corresponding to ideal vacuum state $V_{\rm vac} = I_{4\times4}/2$ (green circle). The cross-quadrature marginals $\{X_1, X_2\}$ and $\{Y_1, Y_2\}$ present two-mode squeezing below the quantum limit in the off-diagonal and diagonal directions. The squeezing angle is given by $\Theta = \frac{1}{2} \arctan[\pm 2V_{13}/|V_{33} - V_{11}|]$[43] and the values are $\mp 44.98°$.

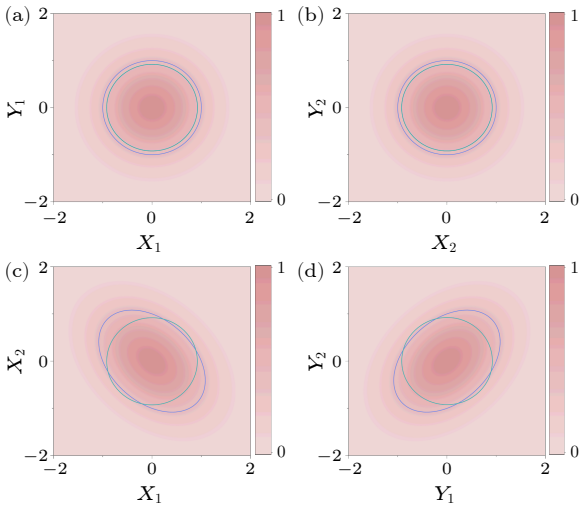

Fig. 3. Normalized projections of the Wigner function of output optical fields' quadrature pairs: [(a), (b)] for the quadratures from the same mode, [(c), (d)] for the cross quadratures. The contours in purple (green) indicate the e^{-1} fall-off from the maximum for our (vacuum) state. The simulation parameters: mechanical angular resonance frequency $\omega_m/2\pi = 5.35$ GHz, mechanical quality factor $Q_m = 1.07 \times 10^8$, optical angular resonance frequencies $\omega_1/2\pi = 198.65$ THz and $\omega_2/2\pi = 191.01$ THz, intrinsic optical quality factors $Q_{\rm in,1} = \omega_1/\kappa_{\rm in,1} = 5.05 \times 10^5$ and $Q_{\rm in,2} = 1.65 \times 10^5$, single photon coupling rates $g_{0,1}/2\pi = 9.77 \times 10^5$ Hz and $g_{0,2}/2\pi = 2.01 \times 10^5$ Hz, coupling ratios $\eta_j = \kappa_{{\rm ex},j}/\kappa_j = 0.5$, temperature $T = 100$ mK, and coherent drive powers $P_{\rm o1} = 8.2$ nW and $P_{\rm o2} = 5$ μW.

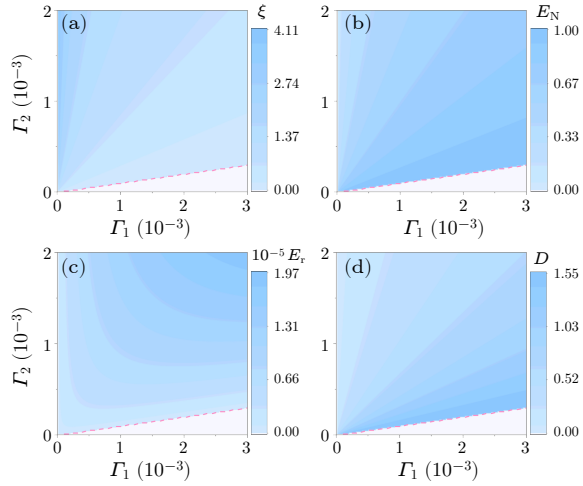

Fig. 4. Entanglement versus the cooperativity Γ_1 and Γ_2 for the same parameters as in Fig. 3. We show entanglement metric ξ derived by the Cauchy–Schwarz criterion in (a), logarithmic negativity $E_{\rm N}$ in (b), entanglement rates $E_{\rm r}$ in (c), and quantum discord D in (d). In each panel, the maximum optical pump powers correspond to $P_{\rm o1} = 0.2$ μW and $P_{\rm o2} = 30$ μW, and the area below the pink dashed line shows the unstable region derived from the Routh–Hurwitz criterion.[45]

The propagating optical fields will get entangled if the value of $\xi \equiv \log_2 \frac{|\langle \hat{d}_1 \hat{d}_2 \rangle|}{\sqrt{\bar{n}_1 \bar{n}_2}}$ exceeds zero in which $\bar{n}_1 \equiv \langle \hat{d}_1^\dagger \hat{d}_1 \rangle$ and $\bar{n}_2 \equiv \langle \hat{d}_2^\dagger \hat{d}_2 \rangle$ are output photon numbers for each field.[45,52–54] As shown in Fig. 4(a), a wide region $\xi > 0$ in

the plane of Γ_j is varied by modulating the driving powers for their respective cavities. The pink dashed line is the boundary between the stable and unstable parameter regions derived by the Routh–Hurwitz criterion,[28,45] which coincides with the boundary of $\xi = 0$. The entanglement of the optical fields leaving the system can be quantified by the logarithmic negativity $E_{\rm N}$,[20,25,52] which sets the upper bound to the number of distillable entanglement bits generated by our source. In Fig. 4(b), the maximum entanglement is obtained with $E_{\rm N} = 1$. Note that the entanglement is robust against temperature.[45] The entanglement rates $E_{\rm r}$ representing the distribution rate of entangled Einstein–Podolsky–Rosen (EPR) pairs is shown in Fig. 4(c),[45] yielding the maximum value $\sim$197 kHz·ebits/s (entanglement rates per second) at $\sim$0.54 MHz bandwidth within experimentally feasible parameter regimes. Recently, the quantum discord D that captures the basic quantum correlations beyond entanglement[20,52,54–56] has shown to be a valuable resource for metrology, e.g., to explain the resilience of quantum illumination.[57] In Fig. 4(d), the maximum quantum discord is obtained to be $D = 1.56$. This suggests that the proposed nanobeam can produce noise-resilient quantum field correlations, demonstrating the potential to be used in quantum metrology, such as quantum illumination in the optical domain.[13,20]

In the application scenarios of quantum networks, the ability to transfer quantum states between different nodes is important. We present the optical quantum state transfer fidelity with our device as an EPR source in an unconditional continuous-variable teleportation scheme.[4,5,58] The state transfer fidelity of an unknown arbitrary coherent squeezed state $|\psi\rangle = |\alpha, r\rangle$ is[43,45]

$$F = [1 + 2^{1-E_{\rm N}} \cosh(2r) + 2^{-2E_{\rm N}}]^{-1/2}, \tag{4}$$

where we have assumed the standard Braunstein–Kimble setup as well as ideal Bell measurements and a lossless classical information transfer. In Fig. 5, the teleportation fidelity can exceed 0.5 in a wide range of Γ_j plane. Two light pink regions for $F \leq 0.5$ correspond to small entanglement that failed to beat the threshold and unstable parameter regimes. Moreover, the fidelity can be improved by enhancing the coupling ratios η_j.[43,59] For instance, the fidelity can obtain its maximum of $\sim$0.65 as the coupling ratios $\eta_1 = \eta_2 = 0.6$ with other parameters kept to be identical.

Working at the nanometer scale dimensions can always result in slight deviations from the intended design parameters. Electron beam lithography dosing, wet chemical etching, resist development, and dry etching which are used to fabricate nanobeams, are typical nanoscale fabrication processes that can introduce these deviations. As such, we analyze the entanglement performance $E_{\rm N}$ with the introduction of structural imperfections over 500 devices.[45] It is shown that the structural parameters that determine the resolved-sideband regime are randomly modified, such that there are 9% of the devices that are not in the resolved-sideband regime for 5 nm overlay accuracy (29.2% for 10 nm). Nevertheless, the maximum entanglement of all the residuals can still exceed 0.9, showing the robustness of the entanglement with considering structural imperfections. Note that the maximum entanglement is obtained near the boundary of the stable region, i.e., $\Gamma_2/\Gamma_1 = 1$, which corresponds to the equal strength of the beam splitter interaction and the parametric downconversion. As shown in Fig. 6, the maximum entanglement can decrease, accompanied by the shrinking of the stable region, and the detailed mathematical derivation can be found in the Supplementary Material.[45]

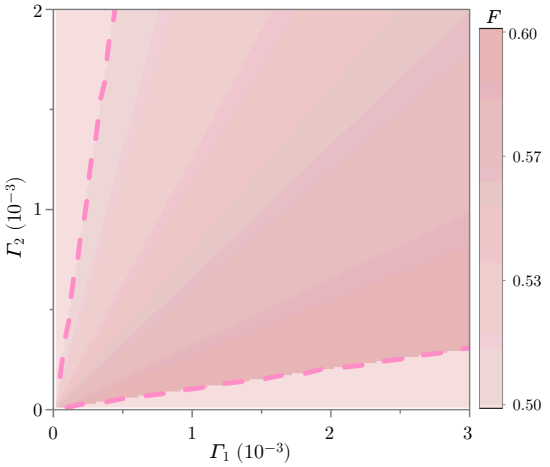

Fig. 5. Teleportation fidelity F for a coherent-squeezed state $|2, 0.5\rangle$ with coherent state amplitude $\alpha = 2$ and squeezing parameter $r = 0.5$. The pink dashed boundary corresponds to $F = 0.5$ and the other parameters are the same as those in Fig. 3.

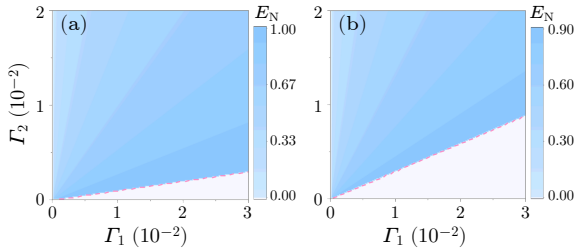

Fig. 6. Entanglement of the device (a) without and (b) with structural imperfections. In the simulations where structural imperfections are introduced, all devices whose maximum entanglement decreases (with the same simulation parameters as in Fig. 3) share the same reason, i.e., the shrinking of the stable region. Therefore, we choose a typical device with the smallest maximum entanglement, $E_{\rm N} = 0.9$, to visualize this phenomenon.

In this work, the Routh–Hurwitz criterion is satisfied when $\Gamma_2/\Gamma_1 > 1$, corresponding to the stronger process of beam splitter interaction than parametric downconversion, as shown in Fig. 1(d). We attribute this phenomenon to that the phonons generated by parametric downconversion can be absorbed by beam splitter interaction instead of accumulating the particles that make the system out of the stable regime. Therefore, for the devices with lowered entanglement (shrinking of the stable region), we can switch their drives so that their maximum entanglement

still obtains $E_{\mathrm{N}} = 1$. It is noteworthy that the state-of-the-art overlay accuracy of electron beam lithography is $\leq 5\,\mathrm{nm}$,[45] which indicates the robustness of our design concerning fabrication processes.

In summary, we present a two-mode optical entanglement source based on triple resonant optomechanical interactions in a single nanobeam. With specific device geometry designed and experimentally feasible parameters simulated, the operating frequency can be tuned flexibly over the telecom band, and the quadrature entanglement of two nondegenerate optical output fields can be obtained. Compared to previous work based on Ref. [21], our results show both advantages of higher integration and enhanced entanglement. Meanwhile, this device can perform teleportation-based quantum state transfer for a typical coherent squeezed state with fidelity exceeding the classical threshold. It is worth noting that improvements in the coupling ratio allow for enhanced entanglement and quantum state transfer fidelity.[43,59] Moreover, considering the structural imperfections in the finite element simulations, the proposed nanobeam shows robustness within the state-of-the-art overlay accuracy of the electron beam lithography.

With enhanced light-matter interactions, this nanoscale device may offer promising avenues toward hybrid quantum systems for versatile quantum state engineering, e.g., multimode microwave-to-optical transducers.[60–64] Wherein one microwave mode might share entanglement with different optical modes as well as multiple microwave-to-optical quantum channels within a single nanobeam can be established. In addition, the current nanobeam contains two resonant telecom-band frequencies. It will be of interest and importance to design structures that can support more telecom-band resonant frequencies simultaneously for versatile nodes in quantum networks.

Acknowledgements. This work was supported by the Sichuan Science and Technology Program (Grant Nos. 2022YFSY0061, 2022YFSY0062, 2022YFSY0063, 2023YFSY0060, 2023YFSY0058, and 2023YFSY0059), the National Key Research and Development Program of China (Grant No. 2022YFA1405900), the National Natural Science Foundation of China (Grant Nos. 92365106, 62005039, 91836102, U19A2076, 12074058, and 62174010), and the Innovation Program for Quantum Science and Technology (Grant Nos. 2021ZD0300701 and 2021ZD0301702).

References

[1] Horodecki R, Horodecki P, Horodecki M, and Horodecki K 2009 *Rev. Mod. Phys.* **81** 865
[2] Wei S H, Jing B, Zhang X Y, Liao J Y, Yuan C Z, Fan B Y, Lyu C, Zhou D L, Wang Y, Deng G W, Song H Z, Oblak D, Guo G C, and Zhou Q 2022 *Laser Photon. Rev.* **16** 2100219
[3] Andersen U L, Gehring T, Marquardt C, and Leuchs G 2016 *Phys. Scr.* **91** 053001
[4] Furusawa A, Sorensen J, Braunstein S, Fuchs C, Kimble H, and Polzik E 1998 *Science* **282** 706
[5] Braunstein S L and Kimble H J 1998 *Phys. Rev. Lett.* **80** 869
[6] Hao S H, Shi H W, Li W, Shapiro J H, Zhuang Q T, and Zhang Z S 2021 *Phys. Rev. Lett.* **126** 250501
[7] Menicucci N C, van Loock P, Gu M L, Weedbrook C, Ralph T C, and Nielsen M A 2006 *Phys. Rev. Lett.* **97** 110501
[8] Ukai R, Iwata N, Shimokawa Y, Armstrong S C, Politi A, Yoshikawa J I, van Loock P, and Furusawa A 2011 *Phys. Rev. Lett.* **106** 240504
[9] Yokoyama S, Ukai R, Armstrong S C, Sornphiphatphong C, Kaji T, Suzuki S, Yoshikawa J I, Yonezawa H, Menicucci N C, and Furusawa A 2013 *Nat. Photon.* **7** 982
[10] Aoki T, Takahashi G, Kajiya T, Yoshikawa J i, Braunstein S L, van Loock P, and Furusawa A 2009 *Nat. Phys.* **5** 541
[11] Lassen M, Sabuncu M, Huck A, Niset J, Leuchs G, Cerf N J, and Andersen U L 2010 *Nat. Photon.* **4** 700
[12] Tan S H, Erkmen B I, Giovannetti V, Guha S, Lloyd S, Maccone L, Pirandola S, and Shapiro J H 2008 *Phys. Rev. Lett.* **101** 253601
[13] Zhang Z S, Mouradian S, Wong F N C, and Shapiro J H 2015 *Phys. Rev. Lett.* **114** 110506
[14] Zhuang Q 2021 *Phys. Rev. Lett.* **126** 240501
[15] Zhuang Q T and Shapiro J H 2022 *Phys. Rev. Lett.* **128** 010501
[16] Aspelmeyer M, Kippenberg T J, and Marquardt F 2014 *Rev. Mod. Phys.* **86** 1391
[17] Barzanjeh S, Xuereb A, Gröblacher S, Paternostro M, Regal C A, and Weig E M 2022 *Nat. Phys.* **18** 15
[18] Rogers B, Lo Gullo N, De Chiara G, Palma G M, and Paternostro M 2014 *Quantum Measurem. Quantum Metrol.* **2** 11
[19] Kurizki G, Bertet P, Kubo Y, Mølmer K, Petrosyan D, Rabl P, and Schmiedmayer J 2015 *Proc. Natl. Acad. Sci. USA* **112** 3866
[20] Barzanjeh S, Redchenko E S, Peruzzo M, Wulf M, Lewis D P, Arnold G, and Fink J M 2019 *Nature* **570** 480
[21] Chen J, Rossi M, Mason D, and Schliesser A 2020 *Nat. Commun.* **11** 943
[22] Palomaki T A, Teufel J D, Simmonds R W, and Lehnert K W 2013 *Science* **342** 710
[23] Ockeloen-Korppi C F, Damskägg E, Pirkkalainen J M, Asjad M, Clerk A A, Massel F, Woolley M J, and Sillanpää M A 2018 *Nature* **556** 478
[24] Kotler S, Peterson G A, Shojaee E, Lecocq F, Cicak K, Kwiatkowski A, Geller S, Glancy S, Knill E, Simmonds R W, Aumentado J, and Teufel J D 2021 *Science* **372** 622
[25] Vitali D, Gigan S, Ferreira A, Böhm H R, Tombesi P, Guerreiro A, Vedral V, Zeilinger A, and Aspelmeyer M 2007 *Phys. Rev. Lett.* **98** 030405
[26] Paternostro M, Vitali D, Gigan S, Kim M S, Brukner C, Eisert J, and Aspelmeyer M 2007 *Phys. Rev. Lett.* **99** 250401
[27] Tian L 2013 *Phys. Rev. Lett.* **110** 233602
[28] Wang Y D and Clerk A A 2013 *Phys. Rev. Lett.* **110** 253601
[29] Ho M, Oudot E, Bancal J D, and Sangouard N 2018 *Phys. Rev. Lett.* **121** 023602
[30] Yu H C, McCuller L, Tse M *et al.* 2020 *Nature* **583** 43
[31] Midolo L, Schliesser A, and Fiore A 2018 *Nat. Nanotechnol.* **13** 11
[32] Chu Y and Gröblacher S 2020 *Appl. Phys. Lett.* **117** 150503
[33] Xu N, Cheng Z D, Tang J D, Lv X M, Li T, Guo M L, Wang Y, Song H Z, Zhou Q, and Deng G W 2021 *Nanophotonics* **10** 2265
[34] González-Tudela A, Reiserer A, García-Ripoll J J, and García-Vidal F J 2024 *Nat. Rev. Phys.* **6** 166
[35] Hill J T, Safavi-Naeini A H, Chan J, and Painter O 2012 *Nat. Commun.* **3** 1196
[36] Buckley S, Radulaski M, Zhang J L, Petykiewicz J, Biermann K, and Vučković J 2014 *Opt. Express* **22** 26498
[37] Grutter K E, Davanço M I, and Srinivasan K 2015 *Optica* **2** 994

[38] Sun F, Yang Y, Li Z, Yang D, Tian H, and Lee C 2022 *Opt. Express* **30** 21764
[39] Wu N, Cui K, Xu Q, Feng X, Liu F, Zhang W, and Huang Y 2023 *Sci. Adv.* **9** eabp8892
[40] Primo A G, Pinho P V, Benevides R, Gröblacher S, Wiederhecker G S, and Alegre T P M 2023 *Nat. Commun.* **14** 5793
[41] Wu N, Cui K, Feng X, Liu F, Zhang W, and Huang Y 2022 *Photonics* **9** 78
[42] Braunstein S L, Fuchs C A, Kimble H J, and van Loock P 2001 *Phys. Rev. A* **64** 022321
[43] Rueda A, Hease W, Barzanjeh S, and Fink J M 2019 *npj Quantum Inf.* **5** 108
[44] Yamaguchi Y, Jeon S W, Song B S, Tanaka Y, Asano T, and Noda S 2015 *J. Opt. Soc. Am. B* **32** 1792
[45] See the Supplementary Material for (i) derivation of the Hamiltonian and dynamics of the system, (ii) covariance matrix of the output optical fields, (iii) entanglement measures of the output optical fields, (iv) robustness of the entanglement against temperature, (v) fidelity of teleportationbased quantum state transfer, (vi) device designs with structural imperfections, (vii) mathematical derivation of the changes of the stable region, (vii) schematic experimental setup.
[46] Barzanjeh S, Abdi M, Milburn G J, Tombesi P, and Vitali D 2012 *Phys. Rev. Lett.* **109** 130503
[47] Cai Q, Fan B, Fan Y, Deng G, Wang Y, Song H, Guo G, and Zhou Q 2023 *Phys. Rev. A* **108** 022419
[48] Quan Q and Loncar M 2011 *Opt. Express* **19** 18529
[49] Fan B, Lv X, Tang T, Deng G, Wang Y, Song H, and Zhou Q 2021 *OSA Continuum* **4** 2998
[50] MacCabe G S, Ren H J, Luo J, Cohen J D, Zhou H Y, Sipahigil A, Mirhosseini M, and Painter O 2020 *Science* **370** 840
[51] Bemani F, Roknizadeh R, Motazedifard A, Naderi M H, and Vitali D 2019 *Phys. Rev. A* **99** 063814
[52] Barzanjeh S, Guha S, Weedbrook C, Vitali D, Shapiro J H, and Pirandola S 2015 *Phys. Rev. Lett.* **114** 080503
[53] Cai Q, Liao J, Shen B, Guo G, and Zhou Q 2021 *Phys. Rev. A* **103** 052419
[54] Rueda A 2021 *Phys. Rev. A* **103** 023708
[55] Pirandola S, Spedalieri G, Braunstein S L, Cerf N J, and Lloyd S 2014 *Phys. Rev. Lett.* **113** 140405
[56] Weedbrook C, Pirandola S, García-Patrón R, Cerf N J, Ralph T C, Shapiro J H, and Lloyd S 2012 *Rev. Mod. Phys.* **84** 621
[57] Weedbrook C, Pirandola S, Thompson J, Vedral V, and Gu M 2016 *New J. Phys.* **18** 043027
[58] Pirandola S, Eisert J, Weedbrook C, Furusawa A, and Braunstein S L 2015 *Nat. Photon.* **9** 641
[59] Sahu R, Qiu L, Hease W, Arnold G, Minoguchi Y, Rabl P, and Fink J M 2023 *Science* **380** 718
[60] Lauk N, Sinclair N, Barzanjeh S, Covey J P, Saffman M, Spiropulu M, and Simon C 2020 *Quantum Sci. Technol.* **5** 020501
[61] Mirhosseini M, Sipahigil A, Kalaee M, and Painter O 2020 *Nature* **588** 599
[62] Arnold G, Wulf M, Barzanjeh S, Redchenko E S, Rueda A, Hease W J, Hassani F, and Fink J M 2020 *Nat. Commun.* **11** 4460
[63] Jiang W T, Sarabalis C J, Dahmani Y D, Patel R N, Mayor F M, McKenna T P, Van Laer R, and Safavi-Naeini A H 2020 *Nat. Commun.* **11** 1166
[64] Weaver M J, Duivestein P, Bernasconi A C, Scharmer S, Lemang M, Thiel T C V, Hijazi F, Hensen B, Gröblacher S, and Stockill R 2023 *Nat. Nanotechnol.* **19** 166